A Computational Model for Repetitive Motion *

Kjeldy A. Haugsjaa, Kamal Souccar, Christopher I. Connolly[†], and Roderic A. Grupen

Laboratory for Perceptual Robotics
Computer Science Department
University of Massachusetts
Amherst, MA

[†]SRI International
Menlo Park, California

Abstract

One of the central issues in the control of articulated limbs is the specification of dynamically feasible trajectories for motion planning. We provide an introduction to discrete configuration space representations and discuss numerical relaxation techniques for computing *harmonic* potential surfaces in these grids. The properties exhibited by harmonic functions which make them well suited to the kind of motion control problems posed in nature are reviewed. Then, an *energy-referenced* controller that makes use of the harmonic potential is formulated to generate and control repetitive motion plans for an articulated mechanism. A possible role for the basal ganglia as a potential-based motor planning mechanism is introduced. Finally, the energy-referenced control scheme is applied to dynamic simulations of the human leg to produce feedback compensated walking gaits. The gaits produced are similar to those derived from human subjects. These preliminary results postulate a simple mechanism for regulating the energy in a biomechanical oscillator in order to produce periodic motor plans.

*This work is supported in part by the National Science Foundation under grants CDA-8922572, IRI-9116297 and IRI-9208920.

Contents

1 Introduction **1**

2 Discrete Configuration Space Representation **2**

3 Harmonic Potentials **3**
3.1 Definition and Properties 4
3.2 Numerical Technique 5

4 Energy-Referenced Control **6**
4.1 Tracking Precision 9
4.2 Orbital Motion 9
4.3 Speculations on a Neural Substrate 10

5 Simulation of the Human Leg **12**
5.1 Terminology 12
5.2 Mechanics 13
5.3 Dynamics 14
5.4 Energy-Referenced Control 14

6 Summary and Discussion **15**

References **18**

A Equation of Motion **22**

B Notes **23**

C Tables **24**

D Figures **26**

1 Introduction

One of the central issues in the control of articulated limbs is the specification of trajectories from one posture to another within constraints imposed by the task. The contexts in which these systems operate vary dramatically, thus constraints also vary. In some cases, collisions with objects in the world must never occur, or joint range limits must not be violated, or at times the quality (kinematic conditioning, actuator load, path smoothness) of the trajectory is critical. This variety of objectives often motivates computational optimization techniques that use models of the task to search for trajectories that meet task specifications. However, these approaches are typically expensive and rely on the existence of complex models that are both complete and correct. As result, trajectory search may lead to brittle strategies that fail in ways that cannot be fully anticipated beforehand, often from seemingly minor deficiencies in the task model. Even if the motion plan is acceptable, it must be compiled into a strategy for driving the actuators so as to track the desired trajectory precisely. The problem is further complicated in dynamical systems, where motion strategies must be feasible in light of the forces and inertias of the limb. This complication is especially relevant in periodic or orbital motion control, a very important class of motion control applications in both natural and robot systems. A theory is required for motion control that incorporates generic constraints, that is dynamically consistent with the articulated structure, and that constitutes a feedback control policy for executing the motion.

In contrast to search techniques, we show how potential fields can be used to formulate "total energy" methods for planning motion. The use of a constant total energy constraint for control has been explored for hopping and juggling robots (Raibert, 1986; Koditschek and Bühler, 1991; Ostrowski and Burdick, 1993). Similarly, the approach described here converges to approximately *constant energy orbits* when released from an initial state. This "energy reference" concept is likewise an attempt to control the system such that the system's total energy is kept constant. The treatment described in this chapter relies on an artificial potential (in the same sense as in (Koditschek, 1991a)). We show how the regulation of constant energy orbits can be achieved by using an energy-referenced feedback loop based on an artificial total energy function (sometimes called a *Hamiltonian* function) for the system.

In this chapter, a harmonic potential field is employed for generating motor plans. Harmonic potentials can be computed with resistive networks, and are "programmable", in the sense that minimum and maximum points only occur at pre-specified locations. This means that goal points and orbit centers can be *pre-programmed* into the potential with the guarantee that they will be the *only* such points in the potential. Obstacles or bounds on the motion are also pre-programmed as maximum points. It is shown how this can be used to construct both convergent (i.e. goal-directed) and repetitive motion plans for a manipulator. In addition, control derived from harmonic potential fields results in *bounded* torques to the joints, and produces compliant, collision-free dynamic behavior. A brief discussion of a recent neurophysiological model (Connolly and Burns, 1993a; Connolly and Burns, 1993b) that postulates a role for the basal ganglia as a potential-based motor planning mechanism is presented. The work described here offers a possible extension of this biological model into the realm of continuous and repetitive motion. The ultimate goal of this work is to incorporate energy and task constraints in a common framework, and to support general classes of *kinodynamic* planning and control.[1] As an example of the generation of repetitive motions, the energy-referenced control scheme is presented for a simulated human leg executing a walking gait.

2 Discrete Configuration Space Representation

The configuration variables, representing independently controllable degrees of freedom in an articulated mechanism, form a natural representation for expressing motion plans. In this chapter, we discuss robot manipulators and dynamic simulations of the human leg. For these types of mechanisms, the configuration variables are the relative angles between adjacent links, $(\theta_0, \theta_1, \ldots, \theta_n)$. The *configuration space* reflects the range of allowable values on these angles. By using these angles, the manipulator can be mapped from a three-dimensional volume to a single point in its configuration space (Lozano-Pérez, 1981). Likewise, a single coordinate in configuration space corresponds to the entire volume in Cartesian space occupied by the manipulator.

In addition to the manipulator, obstacles and goals must also be mapped into the configuration space. Each configuration variable is divided into a number of bins, yielding a discrete configuration space grid or bitmap which describes the entire work space of the limb in terms of its joint angles. Each node in this grid is labeled as either an obstacle, a goal, or accessible free-space. Obstacles typically correspond to geometric constraints for the limb, including other objects in the workspace, joint range limits, or self collision constraints, but in general may represent any constraint on the accessibility of configuration states. If any subset of the Cartesian volume subtended by the mechanism contains an obstacle constraint, then the corresponding configuration space coordinate is labeled inaccessible. Now that a configuration space grid has been constructed which contains information about the obstacles and goals, the path planning problem can be posed as determining an obstacle-avoiding path from a start point to a goal point within the accessible configuration space.

Figure 1 shows the result of a complete mapping for a simple robot workcell. A rectangular object is illustrated inside the workspace of a 2-degree of freedom planar manipulator. Since this manipulator has no joint limits, the configuration space for this problem wraps around at the boundaries. Notice there are multiple goal configurations and there are inaccessible goal configurations embedded within obstacles.

3 Harmonic Potentials

Important properties of controllers,[2] such as stability, convergence, and the existence of spurious equilibria, can be established by examining properties of an underlying potential function. If the potential surface can be shown to have certain properties, then control can be realized as a greedy descent of this surface. This approach leads to robust, closed-loop motor plans that are responsive to variations in the world. In this section, we review these properties as they apply to *harmonic* potentials to justify the application of harmonic potentials to generic motion control tasks. We also introduce a simple numerical method for computing harmonic potentials. In subsequent sections, motor plans are generated for both robot and biological systems that employ harmonic potentials, including periodic motions such as those employed in the human walking gait.

3.1 Definition and Properties

A **potential field** is simply a single-valued function whose gradient is a force applied to the system. An example of a natural potential field is the gravitational potential (mgh), whose gradient, with respect to configuration variable, h (height), is the gravitational force (mg). Gradient descent on **artificial potentials** in configuration space, is often used in robotics as a means of generating torques on the joints of an articulated structure, and yielding responsive, sensor-based robot path plans (Khatib, 1985; Krogh, 1984; Newman and Hogan, 1986; Lyons, 1986; Arkin, 1987; Myers, 1985; Koditschek, 1987a). The way it works is analogous to a marble rolling through a surface of hills and valleys. Unfortunately, the usual formulations of potential fields for path planning do not preclude the spontaneous creation of minima other than the goal. The robot can fall into these minima and achieve a stable configuration short of the goal (Khatib, 1985; Arkin, 1987; Lozano-Pérez, 1982; Canny and Lin, 1990; Barraquand and Latombe, 1991).

Koditschek (Koditschek, 1987b) introduced the formal notion of an admissible potential function for robot path planning. A series of papers (Koditschek, 1989; Koditschek, 1991a; Koditschek, 1991b) established a framework for using artificial potentials to plan and control the trajectories of a mechanical system (e.g. a robot manipulator). Using a total energy formulation, as discussed earlier, "safe" (bounded-torque) controllers can be derived as long as the artificial potential satisfies certain constraints.

Connolly, *et al.* (Connolly et al., 1990), and independently Akishita, *et al.* (Akishita et al., 1990) described the application of harmonic functions to the path-planning problem. **Harmonic functions** are, by definition, solutions to Laplace's equation,

$$\nabla^2\phi = \frac{\partial^2\phi}{\partial q_0^2} + \frac{\partial^2\phi}{\partial q_1^2} + \ldots + \frac{\partial^2\phi}{\partial q_n^2} = 0 \qquad (1)$$

where ϕ is a single-valued function of n independent configuration variables, $\{q_0, q_1, \ldots, q_n\}$. Potential functions that satisfy Laplace's equation are "harmonic potentials." Such potentials generally satisfy the constraints of an admissible potential function, as established by Koditschek, and they exhibit several additional useful properties which make them well suited to motion control applications (Connolly and Grupen, 1993):

correctness — harmonic potentials take on their minimum and maximum values only at goals and obstacles, so a marble rolling on the surface will always reach a goal as long as one is accessible,

completeness — if a path exists, it will be found up to the resolution of the configuration space grid,

robustness — control derived from the harmonic potential responds well to imprecise and/or newly observed constraints, and gradient descent of the harmonic potential minimizes the probability of collisions (Connolly, 1994), and

responsiveness — there is the potential for analog or parallel digital implementations that are capable of forming motion plans very quickly (McCann and Wilts, 1949; Tarassenko and Blake, 1991b; Stan et al., 1994).

Harmonic potentials can be computed over arbitrary, discretized environments such as our configuration space grid, by very fast relaxation techniques. From a biological standpoint, harmonic potentials are useful since they serve as mathematical models for a variety of natural phenomena, including voltages in an electrical network.

3.2 Numerical Technique

As detailed in section 2, the configuration space grid is a discrete (bitmap) representation of the limb workspace. In the most straight-forward implementation of a harmonic function motor planning mechanism, obstacles are set to a fixed maximum potential ($\phi_{obs} = 1$) while goals are grounded ($\phi_{goal} = 0$). The harmonic potential over the remaining free space can be computed using a variety of simple algorithms, most of which can be thought of as forms of repeated averaging or "smoothing" of the function (Burden et al., 1978).

An example of such an algorithm is **Jacobi iteration**. The Jacobi iteration for harmonic functions replaces every non-boundary grid point, $u(x_i, y_j)$, with the average of its neighbors' values *simultaneously*. In two dimensions, this scheme can be written as:

$$u^{(k+1)}(x_i, y_j) = \frac{1}{4}(\quad u^{(k)}(x_{i+1}, y_j) + u^{(k)}(x_{i-1}, y_j) + u^{(k)}(x_i, y_{j+1}) + u^{(k)}(x_i, y_{j-1})) \tag{2}$$

where k is the iteration number. In general, Jacobi iteration replaces the current value with the *average* of neighboring values. With a parallel array of simple processing elements, an iteration over the grid can be accomplished in one parallel step using only one solution variable per processing element, so Jacobi iteration is very efficient on parallel architectures.

Even on sequential computers, relaxation for harmonic potentials is computed very quickly for moderately sized problems. Relaxation times for the examples presented in this chapter are in the millisecond range. Figure 2 provides an example of a 32×32 configuration space grid with geometric obstacles and three goals. Two views of the resulting potential surface are presented; the left panel shows a surface plot and the right panel illustrates the level curves of the surface when viewed from above. Even though the configuration space representation is discrete, we are left with a continuous, smooth surface for control, by interpolating in the space between samples.

4 Energy-Referenced Control

Up to this point, we have introduced harmonic potentials for motion control and reviewed an algorithm for computing them. In this section, we describe a controller in which joint torque commands are obtained from the gradient of a harmonic potential. This control paradigm is illustrated by the generation of repetitive orbital motion. Additionally, the precision with which an industrial-grade robot tracks a reference energy using this paradigm is measured and presented. A role for the basal ganglia in influencing motor control is also suggested.

If we assume we have a perfect dynamic model of the system, that is, we know the masses of the links, and the viscosity and friction at the joints, then each degree of freedom in the system can be "compensated". Compensation allows us to treat the system as a unit mass; in this case, there is no difference between torque and acceleration. This greatly simplifies the required computation. Such a controller is referred to as a **model-based** controller, which computes and sends torque commands to the joint motors of the robot. Under these conditions, we can imagine the system to be a marble of unit mass rolling across the harmonic potential surface. The total energy H in this system is the sum of kinetic and potential energies:

$$H(q,p) = \frac{1}{2}p^2 + \phi(q) \tag{3}$$

where the potential energy is the harmonic potential $\phi(q)$, q is the configuration, and p is the magnitude of the momentum of the particle. Since the mass is 1, the momentum $p = |mv|$ is simply velocity, and $\frac{1}{2}p^2$ is the kinetic energy of the compensated system.

In this formulation, total energy is conserved, that is, $H(q,p)$ ideally stays constant. Hamilton's equations describe the tradeoff between potential and kinetic energy, in terms of position and momentum:[3]

$$\begin{aligned} \dot{q} = &\quad \frac{\partial H}{\partial p} &= p \\ \dot{p} = &\quad -\frac{\partial H}{\partial q} &= -\nabla\phi \end{aligned} \tag{4}$$

These equations describe the motion of a system whose total energy remains constant (a *conservative* system). By these equations, the constant energy constraint requires a reference acceleration for the mechanism, $\dot{p}$, that is equal to the negative gradient of the potential ϕ.

In real mechanisms (robotic and biological), energy is dissipated in joint bearings or in tissue deformation. One might expect the dynamic relation expressed in Equation 4 would slowly "run down" due to these losses in the system. Our solution to this property which is inherent in all real systems is to actively regulate the total energy by adjusting kinetic energy. That is, the desired total energy, H is regulated by introducing or removing kinetic energy — accelerating when energy is too low and decelerating when energy is too high. It will be shown how this *energy-referenced* control scheme can be used to dissipate energy during convergent motion ($H = 0$), or can be used to *overcome* dissipation during orbital motion ($H = E_0$). In this chapter, we are mainly interested with the repetitive motions achieved when total desired energy is positive.

Figure 3 shows the proposed control system. We use closed-loop feedback regulation of the system in which both harmonic potential and kinetic energy influence control. Ideally, the total energy of the system should remain at a reference energy:

$$H_{ref} = \frac{1}{2}(p + \Delta p)^2 + \phi(q) \tag{5}$$

where Δp is the change of momentum required to satisfy the constant energy constraint.

$$\Delta p = [2(H_{ref} - \phi(q))]^{1/2} - p. \tag{6}$$

For a given reference energy, H_{ref} in Figure 3, a compensator, $\psi(\phi(q), p)$, is defined as follows:

$$\begin{aligned} \psi(\phi(q), p) &= [2(H_{ref} - \phi(q))]^{1/2} - p \\ &\quad\ when \ \ ((H_{ref} - \phi(q)) > 0) \\ &= -p \qquad otherwise \end{aligned} \tag{7}$$

In the first case, $H_{ref} > \phi(q)$ and enough energy is introduced in the form of momentum to make up for the system energy deficit. That is, the system's speed (kinetic energy) will have to be increased to keep H_{ref} at its original value. In the second case, however, the system has moved into a region where potentials are too high with respect to the reference, so the system will be braked (the speed lowered), again to keep the total energy constant. In other words, the kinetic energy compensation must behave as a damper to dissipate momentum. In the examples presented, kinetic energy is added or removed only along the current trajectory.

Under these conditions, the reference acceleration of the system is:

$$\ddot{q}_{ref} = -\nabla\phi \ + \ G_{KE}\ [\psi(\phi(q), p)] \tag{8}$$

where G_{KE} is the derivative feedback gain that weighs the relative influence of kinetic and potential energy in the system.

As mentioned earlier, obstacle potentials are fixed at a uniform value, $\phi_{obs} = 1$, which is the maximum potential energy in the system. Under the energy-referenced control scheme, the system energy is never allowed to exceed this obstacle potential. If errors in the energy-referenced controller are neglected, then as long as $H_{ref} < \phi_{obs}$, the system cannot encounter a configuration space obstacle with non-zero velocity. In general, level sets of ϕ at $\phi = H_{ref}$ bound the motion of the system. The right panel of figure 2 illustrates the level sets of ϕ for that motion planning problem. As the reference energy H_{ref} is set to smaller values, the system becomes constrained by smaller areas surrounding the goal configurations.

4.1 Tracking Precision

Just as in classical feedback compensators, the precision and settling time of the system as it seeks the reference energy are functions of the control gains for proportional and derivative feedback. To provide a data point regarding the stability and tracking performance in a real system, the energy-referenced control scheme was implemented on a GE-P50 robot arm. The shoulder and the elbow of this robot were controlled forming a 2 degree-of-freedom planar arm. The P50 is a relatively massive industrial robot for which only coarse feedforward dynamic compensators are available. This is a common deficiency in most real systems (and perhaps biological systems as well), the effect of which is to introduce unmodeled disturbances. Figure 4 shows an example trajectory derived from this system. The left panel depicts the configuration space of the robot where the open square again represents the goal ($\phi_{goal} = 0$) and dark filled squares represent obstacles ($\phi_{obs} = 1$). The right panel shows the energy levels measured during the motion sequence. The example is typical of real systems and illustrates that relatively small tracking errors are possible for suitable control parameters.

4.2 Orbital Motion

When H_{ref} is set to 0, the system configuration reaches one of the available goal configurations (where the potential energy is 0) and stops (kinetic energy is 0). Since $\phi_{goal} = 0$, this represents a kind of goal-directed (or *convergent*) motion. Orbital motion is achieved by setting H_{ref} to some value between ϕ_{goal} and ϕ_{obs}. This results in an approximately constant energy trajectory that is bounded by the corresponding equipotential set of ϕ. The system becomes trapped within the basin of attraction of a goal. In other words, if we try to keep H_{ref} at a constant, positive value, the system will tend to orbit the goal (minimum) points of ϕ, the harmonic potential. Figure 4 depicts such an orbit in the motion sequence derived from our P50 robot arm. The balance of kinetic and potential energy maintains the elliptical motion illustrated. This representation can be used to "plan" simple repetitive motions such as turning a crank or stepping in a legged system, as we shall see in section 5.

4.3 Speculations on a Neural Substrate

The motion planning approach described in the preceding sections relies on a harmonic potential to guide and restrict the movement of a limb. Harmonic (or nearly harmonic) potentials arise in a variety of physical phenomena, such as, diffusion, electrostatics, fluid flow, and especially resistive networks. In particular, we can replace the grid of parallel processors described in section 2 with a grid of resistors, and still obtain a harmonic potential. It seems natural to ask whether it is plausible for some neural process to exploit these phenomena for motor planning.

Some recent speculations on the function of the basal ganglia (Houk et al., 1995) suggest that these nuclei are involved in context-driven generation of motor plans, that is, they associate sensory cues and environmental context with an appropriate action or goal. One relevant feature of the basal ganglia is that they are topographically organized. In primates, the striatum (the "input" area for the basal ganglia) appears to be subdivided into regions corresponding to the face and limbs (Alexander and Crutcher, 1990). Basal ganglia involvement in motor planning seems likely given the symptoms of Parkinson's (e.g., festination, rigidity) and Huntington's diseases (e.g., chorea, involuntary twitching) both of which severely affect the basal ganglia. One view of basal ganglia function, then, is that they receive sensory information (context) from the cortex, and help select appropriate actions and goals based on that context.

A recent theory of striatum function (Connolly and Burns, 1993a; Connolly and Burns, 1995) suggests that a resistive network can serve as a model for the motor-planning role of the striatum. An additional motivation for this suggestion is recent evidence of dye coupling (Onn and Grace, 1994; Cepeda et al., 1989) and gap junctions (Kita et al., 1990) among cells in the striatum. Dye-coupling and the presence of gap junctions both suggest that striatal neurons could have direct cell-to-cell connections – probably at the dendrites – through which small molecules, cytoplasm, and electrical current can flow. This allows the network of cells in the striatum to be thought of as a resistive network. Even when they are not firing, striatal cells are known to exhibit fluctuations in their membrane potentials (so-called "subthreshold activity" (Houk et al., 1995)). Striatal projection neurons (which comprise about 95% of the striatum), are usually quiet. A large amount of cortical excitation drives striatal neurons into an "up" state, which is at a membrane potential just *below* the firing threshold. These neurons are also known to exhibit a "down" state. For motor planning, it is possible that these two states represent information about obstacle and goal configurations (the task context), in which case resistive coupling among these cells would rapidly give rise to a harmonic potential expressed as the membrane potentials of cells in a limb-related region of striatal tissue. This in turn could be used as part of the motor planning process for that limb.

As stated, the theory in (Connolly and Burns, 1993a) represents pure path planning. That is, motion is planned as a gradient descent on a harmonic potential, without considering the dynamics of the limb. A natural extension to this theory would incorporate the results described in this chapter, using the physical properties of the limb (e.g., mass, joint viscosity) in the motion planning process. One consequence of this theoretical treatment is an explanation for festination (the "running-down" seen in Parkinson's patients): The inability to maintain potentials in the striatum during repetitive motion (e.g. walking or handwriting) results in progressively smaller orbits, until the motion ceases altogether. This effect can be achieved in a robotic system by allowing the goal potential to "float upward", until it reaches the same value as the obstacle potential. With a positive reference energy H_{ref}, this results in progressively smaller orbits, until the motion ceases altogether, at which point the system is rigid. The rigidity observed in a robotic system at this point is analogous to rigidity seen in Parkinsons patients: The limb is plastic, and upon being moved to a different configuration, will stay there. One advantage to the scheme discussed in this chapter is that it does not directly specify positions or velocities for a limb. Instead, it relies on delivering torques to the joints to influence movement in a *compliant* way (that is, the limb can yield to external forces if necessary). This is more consistent with observations of force-related responses in striatal neurons (Wickens, 1993).

5 Simulation of the Human Leg

Human locomotion is naturally expressed as an orbital gait pattern. We postulate that natural walking gaits consist of a synergy between constraint satisfaction and a dynamically feasible motor plan. The constraints, in this case, require that the trajectory does not exceed joint limits and that the total system energy is regulated so as to further restrict the set of achievable configurations. This section introduces a simple kinematic and dynamic model of the human leg and generates a periodic gait pattern using the energy-referenced control scheme. The performance of the controller is compared to data derived from a human subject.

5.1 Terminology

The term "gait pattern" is used here to refer to the periodic leg trajectory generated when people move forward over smooth terrain. More specifically, this chapter focuses on patterns of *walking* gaits. Figure 5 illustrates a common cycle in a walking gait. This diagram is referred to as an "angle-angle" diagram in biomechanics literature (Enoka et al., 1982), and is essentially equivalent to a trajectory through configuration space. The time history of the hip and knee configuration characterize the gait pattern, so angle-angle diagrams are helpful in evaluating and comparing gaits. Knee and ankle diagrams are also often used. The usefulness of angle-angle diagrams for therapeutic means are noted by (Rosenbaum, 1991). They will be used in this paper to evaluate and compare our simulated monoped gait to that of a real human.

Figure 5 identifies critical events in a walking gait pattern. Knee flexion is indicated by downward motion and knee extension is indicated by upward motion in the angle-angle plots. Likewise, hip rotation forward is to the right and backward rotation is to the left. Toe-Off (TO) is the point when a given foot leaves the ground at one of the relatively extreme knee extensions. After TO, the leg is in the swing phase until heel contact (HC), where the knee angle is almost fully extended. At this point, the leg enters the stance phase of the cycle where it remains until TO again. The stance phase is the part of the orbit between HC and TO, seen by the "dip" at the top of the cycle in the angle-angle diagrams. One complete walking stride is defined as the period between successive TOs. Thus, a stride is one orbit in the counter-clockwise direction from TO to TO. The range of motion of both joints is indicated by the total area covered by the cycle.

5.2 Mechanics

We use a three degree-of-freedom, planar mechanism to approximate the human leg as illustrated in Figure 6. The thigh, shank, and foot, links 0, 1, and 2 respectively, are all modeled, and the motion of the leg is restricted to the sagittal plane (xy plane). Each of the three links is characterized by a point mass located at the center of mass and a rotational moment of inertia. The dynamic parameters are defined as those of the subject used in the walking trial example found in (Winter, 1990). The mass moments of inertia were calculated using the data for the average radii of gyration specified in (Winter, 1990). The values associated with the inertial parameters are summarized in Table 1.

The simulation also models the passive elasticity in each joint since this is known to play a significant role in managing the motion of the skeleton (Winter, 1990). The complex interconnection of limb segments in a human body involves many muscles, ligaments, tendons, and skin crossing each joint. A passive joint moment arises from the deformation of all these tissues. Elastic moments about the hip and the knee were modeled from measurements of such moments *in vivo* (Yoon and Mansour, 1982; Mansour and Audu, 1986). Exponential functions were fitted to this experimental data, for both joint flexion and extension, and a linear function was used in the midrange joint values, when the elastic moment is near 0. A similar elasticity function was determined for the ankle joint. These functions represent the relationship between the passive hip, knee, and ankle moment and the respective joint angles, as shown in Figure 7. Clearly as a joint nears its limit, the passive elastic moment increases greatly. The elastic moment of the hip is strongly dependent on the position of both knee and hip (it should be noticeably more difficult to rotate your hip forward as your knee is further extended). As result we use one of three functions, indexed by knee angle, to model the elastic moments of the hip.

5.3 Dynamics

The dynamic model employed by our simulated monoped is given by the following,

$$\tau = M(\theta)\,\ddot{\theta} + C(\theta,\dot{\theta}) + G(\theta) + E(\theta). \tag{9}$$

$M(\theta)$ is the 3×3 inertia tensor for the leg, $C(\theta,\dot{\theta})$ expresses Coriolis and centrifugal loads, $G(\theta)$ represents the gravity loads, and $E(\theta)$ is a vector which accounts for moments from the natural elasticity of tissues surrounding the joints of a human leg. Equation 9 transforms the state of motion, $(\theta,\dot{\theta})$, and the desired acceleration in the mechanism, $\ddot{\theta}$, into the torque load τ at each joint in the mechanism. Likewise, the state of motion $(\theta,\dot{\theta})$ and the applied torque yield the acceleration in the leg,

$$\ddot{\theta} = M^{-1}[\tau - C(\theta,\dot{\theta}) - G(\theta) - E(\theta)]. \tag{10}$$

The Newton-Euler method was used to obtain the dynamic equation of motion. The parameters of the equation of motion are completely defined in Appendix A.

5.4 Energy-Referenced Control

Figure 8 shows an example of an orbit generated by the energy-referenced controller driving the simulated leg. The dark regions again represent obstacles assigned a potential of $\phi_{obs} = 1$. These boundary obstacles represent the joint angle limits of the leg. The open squares represent goals assigned a potential of $\phi_{goal} = 0$. The energy reference, H_{ref}, is defined to be 0.8. The energy-referenced controller manages the hip, θ_0 and the knee, θ_1, while the ankle is subject to the passive elastic moments exclusively. The results presented here are derived from 10 full simulated strides of the monoped.

Figure 9 presents a comparison with a walking stride derived from the human subject reported in (Winter, 1990) and the energy-referenced controller acting on the dynamic simulation of Winter's subject. The two angle-angle plots give the general impression that they share a similar pattern of motion. Both execute a stable, cyclic motion pattern with the characteristic dip during the stance phase, and both orbits cover a similar area.

6 Summary and Discussion

In this chapter, we introduced the configuration space representation and motivated a procedure for mapping task geometry to accessibility constraints for articulated limbs. A procedure for transforming geometric motion constraints into the harmonic potential was presented. As result of the properties of harmonic potential functions, we formulated an energy-referenced controller capable of sustaining periodic, orbital motion and demonstrated such orbital motion in robot systems. A role for the basal ganglia in biological motor control was postulated. We then introduced a kinematic and dynamic model of the human leg and applied the energy-referenced control paradigm to this system. We demonstrated that this approach can yield qualitatively similar behavior to that observed in the human walking gait. The results of this exercise lend some credibility to the notion that motion plans should deal with external constraints in a manner that is consistent with the underlying dynamics of physical systems.

Underlying this work is the presumption that human motor control has evolved to optimize energetic efficiency and so has exploited the dynamics of the "plant" (arm, leg, etc). Our objective has been to apply engineering principles to implement a controller that can generate convergent and periodic motions while responding to systems of dynamic constraints. In a sense, we have formulated a natural oscillator in the configuration of the leg, constrained initially by intrinsic kinematics, and subsequently "shaped" by the placement of task specific constraints (goals and obstacles) and control parameters (H_{ref}).

One instance in which the decision of where to place goals and obstacles proved critical surfaced in the course of experimental work. In robot control applications, it is prudent to treat joint angle limits as obstacles and thus to guarantee that the trajectory plan will not violate them. Moreover, full knee extension is a kinematic singularity implying that impact at ground strike with an extended knee transmits large forces into the joints. Both circumstances lead to expensive failures in robot applications. Walking gaits in humans, however, clearly emphasize energetic efficiency rather than joint limits or kinematic singularities. During the stance phase, the knee is very nearly fully extended. This makes sense in that during the load carrying phase of the stride, this posture effectively transfers the load from the musculature into the skeleton, but only at the expense of knee and hip joints. In recent work, we have begun to formulate adaptive mechanisms for optimizing performance by modulating the shape of the harmonic potential (Coelho et al., 1996). We propose these mechanisms as a means of acquiring skillful and efficient motor policies in a manner consistent with intrinsic kinematic and dynamic properties.

Although there are many overall similarities in the gait patterns presented here, if we turn up the microscope, there are noteworthy variations. As Figure 9 illustrates, the simulated knee is not extending as much as the actual human's knee, and it is flexing too much. This is possibly due to an aversion of our controller to joint limits as described in the previous paragraph. As for the hip angle, it is rotated forward slightly for the entire stride — rotating forward excessively before HC and then not rotating backward quite enough for TO. Also, the "dip" at the top of each angle-angle diagram, which represents the stance (or load carrying) phase, is fairly different in shape. It is possible that this difference is the result of ground reaction forces experienced by human subjects, but not modeled in the simulator. The effect of a periodic external perturbation on the orbit can be a primary influence on the shape of the kinodynamic orbit. Moreover, the shape of this periodic forcing function, a property that depends on the shape of the foot, is likewise, potentially critical. The simulated leg does not experience these loads. This fact could account for many of the differences observed. Specifically, the tendency of the orbit to be skewed forward might be due to the lack of a backward directed friction force during the support phase.

From a technical perspective, several important questions regarding the application of energy-referenced controllers remain open. For instance, kinetic energy is currently added or removed from the system along the current trajectory, but there are a continuum of other alternatives. It may be possible to address phase space constraints, e.g., maintenance of a particular phase relationship between joint velocities, or to excite fundamental oscillatory modes of the device. This may provide a mechanism for strategically shaping the orbit for a task.

Finally, although it is premature to draw any strong conclusions with respect to the proposed role of the basal ganglia in motor control, we have shown that dynamic oscillators driven by conservative potentials form a compelling basis for periodic, kinodynamic behavior. The value of harmonic potentials in robot systems is manifold: from their computational characteristics, collision avoidance properties, robustness with respect to cumulative information, their ability to incorporate generic constraints, and the absence of local minima. Moreover, the variety of natural processes captured by Laplace's equation and the potential to exploit massive parallelism when computing harmonic potentials offers evidence (albeit circumstantial) that this process could reside in the basal ganglia.

References

Akishita, S., Kawamura, S., and Hayashi, K. (1990). Laplace potential for moving obstacle avoidance and approach of a mobile robot. In *1990 Japan-USA Symposium on Flexible Automation, A Pacific Rim Conference*, pages 139–142.

Alexander, G. E. and Crutcher, M. D. (1990). Functional architecture of basal ganglia circuits: neural substrates of parallel processing. *Trends in Neurosciences*, 13(7):266–271.

Arkin, R. C. (1987). Towards cosmopolitan robots: Intelligent navigation in extended man-made environments. Technical Report 87-80, COINS Department, University of Massachusetts.

Barraquand, J. and Latombe, J.-C. (1991). Robot motion planning: A distributed representation approach. *International Journal of Robotics Research*, 10(6):628–649.

Burden, R. L., Faires, J. D., and Reynolds, A. C. (1978). *Numerical Analysis.* Prindle, Weber and Schmidt, Boston.

Canny, J. F. and Lin, M. C. (1990). An opportunistic global path planner. In *Proceedings of the 1990 IEEE International Conference on Robotics and Automation*, pages 1554–1559.

Cepeda, C., Walsh, J. P., Hull, C. D., Howard, S. G., Buchwald, N. A., and Levine, M. S. (1989). Dye-coupling in the neostriatum of the rat: I. modulation by dopamine-depleting lesions. *Synapse*, 4:229–237.

Coelho, J. A., Sitaraman, R. K., and Grupen, R. A. (1996). Parallel optimization of motion controllers via policy iteration. In *Proceedings of the 1996 Advances in Neural Information Processing Systems*, pages 996–1002.

Connolly, C. and Burns, J. B. (1995). A state-space striatal model. In Houk, J., Davis, J., and Beiser, D., editors, *Models of Information Processing in the Basal Ganglia.* MIT Press.

Connolly, C. I. (1994). Harmonic functions and collision probabilities. In *Proceedings of the 1994 IEEE International Conference on Robotics and Automation*, pages 3015–3019. IEEE.

Connolly, C. I. and Burns, J. B. (1993a). A model for the functioning of the striatum. *Biological Cybernetics*, 68(6):535–544.

Connolly, C. I. and Burns, J. B. (1993b). A new striatal model and its relationship to basal ganglia diseases. *Neuroscience Research*, 16:271–274.

Connolly, C. I., Burns, J. B., and Weiss, R. (1990). Path planning using Laplace's Equation. In *Proceedings of the 1990 IEEE International Conference on Robotics and Automation*, pages 2102–2106. IEEE.

Connolly, C. I. and Grupen, R. (1992). Applications of harmonic functions to robotics. Technical Report 92-12, COINS Department, University of Massachusetts.

Connolly, C. I. and Grupen, R. A. (1993). The applications of harmonic functions to robotics. *Journal of Robotic Systems*, 10(7):931–946.

Enoka, R. M., Miller, D. I., and Burgess, E. M. (1982). Below-knee amputee running gait. *American Journal of Physical Medicine*, 61(2):66–84.

Houk, J., Davis, J., and Beiser, D., editors (1995). *Models of Information Processing in the Basal Ganglia.* MIT Press.

Khatib, O. (1985). Real-time obstacle avoidance for manipulators and mobile robots. In *Proceedings of the 1985 IEEE International Conference on Robotics and Automation*, pages 500–505. IEEE.

Kita, H., Kosaka, T., and Heizmann, C. W. (1990). Parvalbumin-immunoreactive neurons in the rat neostriatum: A light and electon microscope study. *Brain Research*, 536:1–15.

Koditschek, D. E. (1987a). Exact robot navigation by means of potential functions: Some topological considerations. In *Proceedings of the 1987 IEEE International Conference on Robotics and Automation*, pages 1–6. IEEE.

Koditschek, D. E. (1987b). Exact robot navigation by means of potential functions: Some topological considerations. In *Proceedings of the 1987 IEEE International Conference on Robotics and Automation*, pages 1–6. IEEE.

Koditschek, D. E. (1989). The application of total energy as a lyapunov function for mechanical control systems. In *Dynamics and Control of Multibody Systems*, volume 97 of *Contemporary Mathematics*, pages 131–157. American Mathematical Society.

Koditschek, D. E. (1991a). The control of natural motion in mechanical systems. *Journal of Dynamic Systems, Measurement, and Control*, 113:547–551.

Koditschek, D. E. (1991b). Some applications of natural motion control. *Journal of Dynamic Systems, Measurement, and Control*, 113:552–557.

Koditschek, D. E. and Bühler, M. (1991). Analysis of a simplified hopping robot. *International Journal of Robotics Research*, 10(6):587–605.

Krogh, B. H. (1984). A generalized potential field approach to obstacle avoidance control. In *Robotics Research: The Next Five Years and Beyond*. Society of Manufacturing Engineers.

Lozano-Pérez, T. (1981). Automatic planning of manipulator transfer movements. *IEEE Transactions on Systems, Man, and Cybernetics*, SMC-11(10):681–698.

Lozano-Pérez, T. (1982). Robotics (correspondent's report). *Artificial Intelligence*, 19(2):137–143.

Lyons, D. (1986). Tagged potential fields: An approach to specification of complex manipulator configurations. In *Proceedings of the 1986 IEEE International Conference on Robotics and Automation*, pages 1749–1754. IEEE.

Mansour, J. M. and Audu, M. L. (1986). The passive elastic moment at the knee and its influence on human gait. *Journal of Biomechanics*, 19(5):369–373.

McCann, G. D. and Wilts, C. H. (1949). Application of electric-analog computers to heat-transfer and fluid-flow problems. *Journal of Applied Mechanics*, 16(3):247–258.

Myers, J. K. (1985). Multiarm collision avoidance using the potential field approach. In *Space Station Automation*, pages 78–87. SPIE.

Newman, W. S. and Hogan, N. (1986). High speed robot control and obstacle avoidance using dynamic potential functions. Technical Report TR-86-042, Philips Laboratories.

Onn, S.-P. and Grace, A. A. (1994). Dye coupling between rat striatal neurons recorded in vivo: Compartmental organization and modulation by dopamine. *Journal of Neurophysiology*, 71(5):1917–1934.

Ostrowski, J. P. and Burdick, J. W. (1993). Designing feedback algorithms for controlling the periodic motions of legged robots. In *Proceedings of the 1993 IEEE International Conference on Robotics and Automation*, pages 254–260. IEEE.

Raibert, M. H. (1986). *Legged Robots that Balance*. MIT Press, Cambridge, MA.

Rosenbaum, D. A. (1991). *Human Motor Control*. Academic Press, Inc., San Diego, CA.

Stan, M. R., Burleson, W. P., Connolly, C. I., and Grupen, R. A. (1994). Analog vlsi for robot path planning. *Journal of VLSI Signal Processing*, 8(1):61–73.

Tarassenko, L. and Blake, A. (1991a). Analogue computation of collision-free paths. In *Proceedings of the 1991 IEEE International Conference on Robotics and Automation*, pages 540–545. IEEE.

Tarassenko, L. and Blake, A. (1991b). Analogue computation of collision-free paths. In *Proceedings of the 1991 IEEE International Conference on Robotics and Automation*, pages 540–545. IEEE.

Wickens, J. (1993). *A Theory of the Striatum*, volume 7 of *Pergamon studies in neuroscience.* Pergamon Press, New York.

Winter, D. A. (1990). *Biomechanics and Motor Control of Human Movement.* John Wiley and Sons, Inc., New York, NY.

Yoon, Y. S. and Mansour, J. M. (1982). The passive elastic moment at the hip. *Journal of Biomechanics*, 15(12):905–910.

A Equation of Motion

The following is the dynamic equation of motion for the three link manipulator.

$$\tau = M(\theta)\,\ddot{\theta} + C(\theta,\dot{\theta}) + G(\theta) + E(\theta)$$

where:

$$M(\theta) = \begin{bmatrix} M_{00} & M_{01} & M_{02} \\ M_{10} & M_{11} & M_{12} \\ M_{20} & M_{21} & M_{22} \end{bmatrix} \quad C(\theta,\dot{\theta}) = \begin{bmatrix} C_0 \\ C_1 \\ C_2 \end{bmatrix} \quad G(\theta) = \begin{bmatrix} G_0 \\ G_1 \\ G_2 \end{bmatrix} \quad E(\theta) = \begin{bmatrix} E_0 \\ E_1 \\ E_2 \end{bmatrix}$$

$$\begin{aligned}
M_{22} &= I_2 + I_{cm2} \\
M_{21} &= M_{22} + l_1\, l_{cm2}\, m_2\, c_2 \\
M_{20} &= M_{21} + l_0\, l_{cm2}\, m_2\, c_{12} \\
M_{12} &= M_{21} \\
M_{11} &= M_{12} + I_1 + I_{cm1} + l_1^2\, m_2 + l_1\, l_{cm2}\, m_2\, c_2 \\
M_{10} &= M_{11} + (l_0\, l_{cm1}\, m_1 + l_0\, l_1\, m_2)\, c_1 + l_0\, l_{cm2}\, m_2\, c_{12} \\
M_{02} &= M_{20} \\
M_{01} &= M_{10} \\
M_{00} &= M_{01} + I_0 + I_{cm0} + l_0^2\,(m_1 + m_2) + (l_0\, l_{cm1}\, m_1 + l_0\, l_1\, m_2)\, c_1 + l_0\, l_{cm2}\, m_2\, c_{12} \\
C_2 &= l_1\, l_{cm2}\, m_2\, s_2\, (\dot{\theta}_0^2 + 2\,\dot{\theta}_0\,\dot{\theta}_1 + \dot{\theta}_1^2) \;+\; l_0\, l_{cm2}\, m_2\, s_{12}\,\dot{\theta}_0^2 \\
C_1 &= (l_0\, l_{cm1}\, m_1 + l_1\, m_2)\, s_1\,\dot{\theta}_0^2 \;-\; l_1\, l_{cm2}\, m_2\, s_2\,(2\,\dot{\theta}_0\,\dot{\theta}_2 + 2\,\dot{\theta}_1\,\dot{\theta}_2 + \dot{\theta}_2^2) \\
&\qquad + l_0\, l_{cm2}\, m_2\, s_{12}\,\dot{\theta}_0^2 \\
C_0 &= -\,(l_0\, l_{cm1}\, m_1 + l_1\, m_2)\, s_1\,(2\,\dot{\theta}_0\,\dot{\theta}_1 + \dot{\theta}_1^2) \;-\; l_1\, l_{cm2}\, m_2\, s_2\,(2\,\dot{\theta}_0\,\dot{\theta}_2 + 2\,\dot{\theta}_1\,\dot{\theta}_2 + \dot{\theta}_2^2) \\
&\qquad -\, l_0\, l_{cm2}\, m_2\, s_{12}\,(2\,\dot{\theta}_0\,\dot{\theta}_1 + 2\,\dot{\theta}_0\,\dot{\theta}_2 + 2\,\dot{\theta}_1\,\dot{\theta}_2 + \dot{\theta}_1^2 + \dot{\theta}_2^2) \\
G_2 &= g\, l_{cm2}\, m_2\, s_{012} \\
G_1 &= G_2 + g\,(l_{cm1}\, m_1 + l_1\, m_2)\, s_{01} \\
G_0 &= G_1 + g\,(l_{cm0}\, m_0 + l_0\, m_1 + l_0\, m_2)\, s_0 \\
E_2 &= \text{Refer to bottom panel of figure 7.} \\
E_1 &= \text{Refer to middle panel of figure 7.} \\
E_0 &= \text{Refer to top panel of figure 7.}
\end{aligned}$$

and in general: $s_{ijk} = sin(\theta_i + \theta_j + \theta_k)$ $\quad c_{ijk} = cos(\theta_i + \theta_j + \theta_k)$.

B Notes

1 That is, motor planning which incorporates both geometric and dynamic aspects of the motion.

2 For a robot, this is the controlling hardware and software required to execute a trajectory.

3 Together, these are known as the *phase space* of the system. Configuration space (position) is a subset of phase space.

C Tables

Table 1: Kinematic and Dynamic Parameters of the Human Subject.

Link	Length (m)	Center of Mass (m)	Mass (kg)	Moment of Inertia ($kg * m^2$)
Thigh (0)	0.36	0.16	5.67	0.079
Shank (1)	0.39	0.17	2.34	0.032
Foot (2)	0.24	0.12	0.82	0.010

Note that values for the location of the center of mass are lengths from the proximal end of each segment.

List of Figures

1 Configuration space for a 2 degree of freedom, planar arm. 26

2 Left: Converged plot of a harmonic potential function with 3 goals; Right: level sets of harmonic potential, where white is the obstacle potential ($\phi_{obs} = 1$) and black is the goal potential ($\phi_{goal} = 0$). 27

3 Energy-referenced controller. 27

4 GE-P50 constant-energy orbit. Left: configuration space; Right: energy levels. 28

5 Typical angle-angle diagram of a walking gait. 28

6 Geometry of the Simulated Human Leg. 29

7 Elastic Moment about the hip, knee, (adapted from (Yoon and Mansour, 1982; Mansour and Audu, 1986)) and ankle joints. 30

8 Monoped constant-energy orbit in configuration space. 31

9 Comparison of the angle-angle diagram for the human subject and the dynamically equivalent leg simulation. 31

D Figures

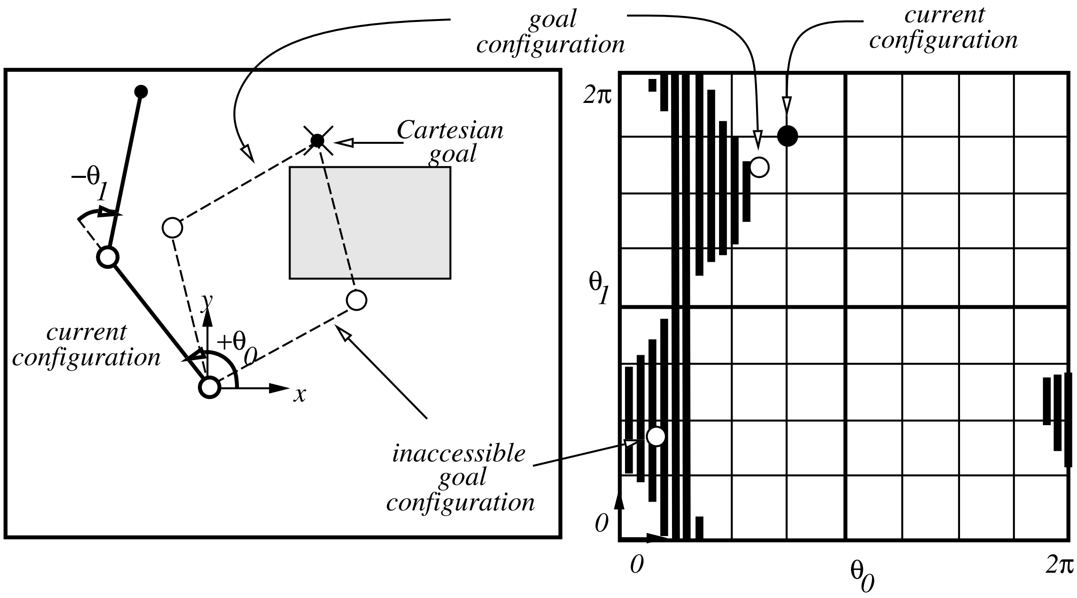

Figure 1: Configuration space for a 2 degree of freedom, planar arm.

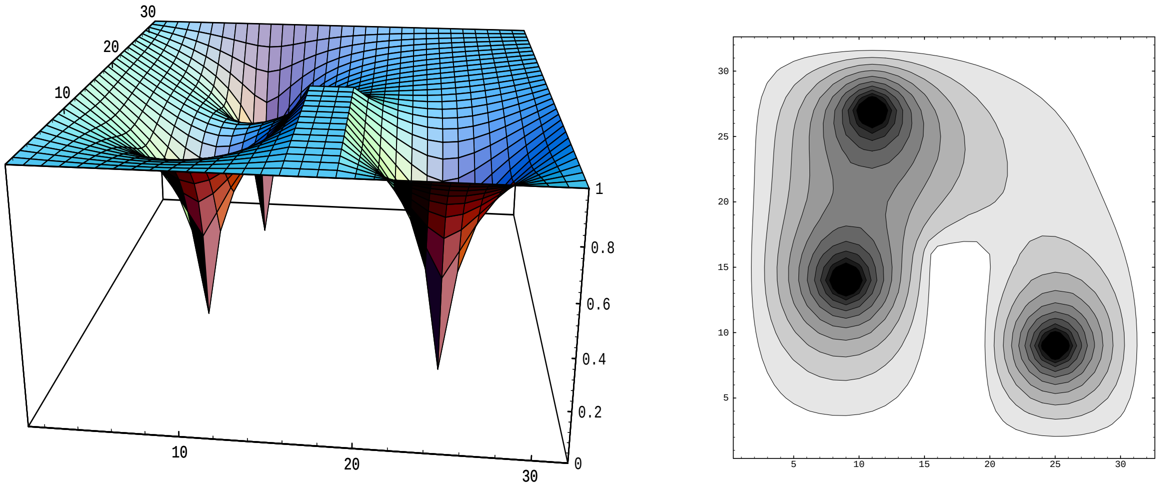

Figure 2: Left: Converged plot of a harmonic potential function with 3 goals; Right: level sets of harmonic potential, where white is the obstacle potential ($\phi_{obs} = 1$) and black is the goal potential ($\phi_{goal} = 0$).

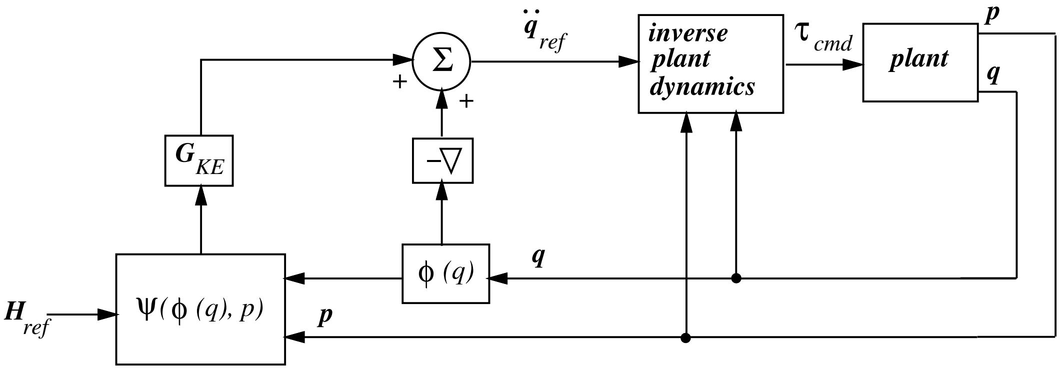

Figure 3: Energy-referenced controller.

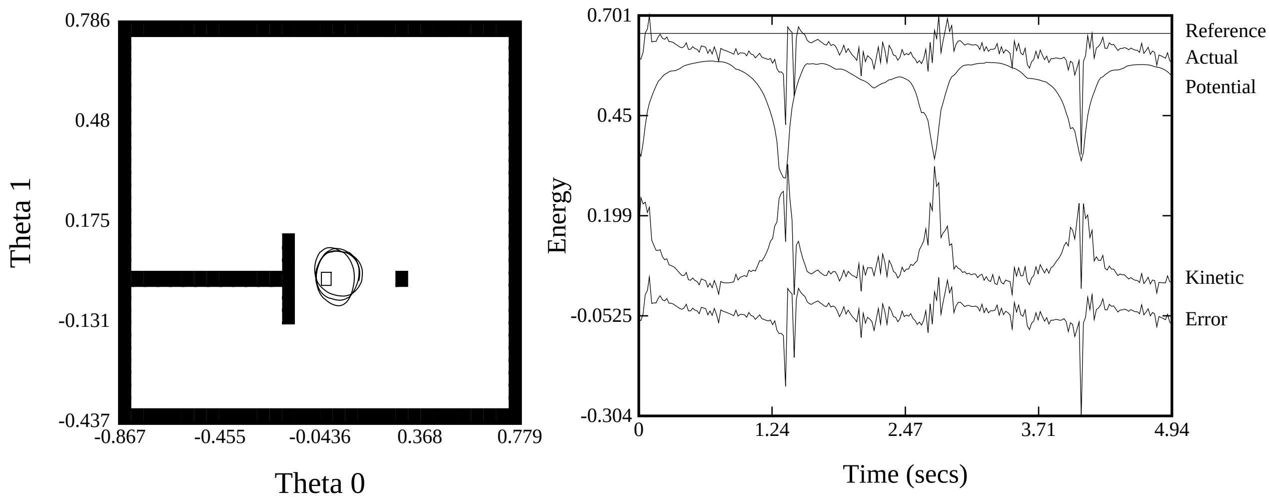

Figure 4: GE-P50 constant-energy orbit. Left: configuration space; Right: energy levels.

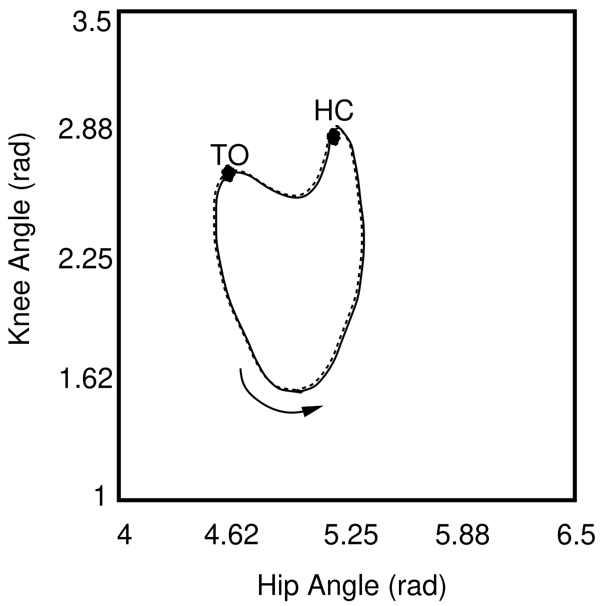

Figure 5: Typical angle-angle diagram of a walking gait.

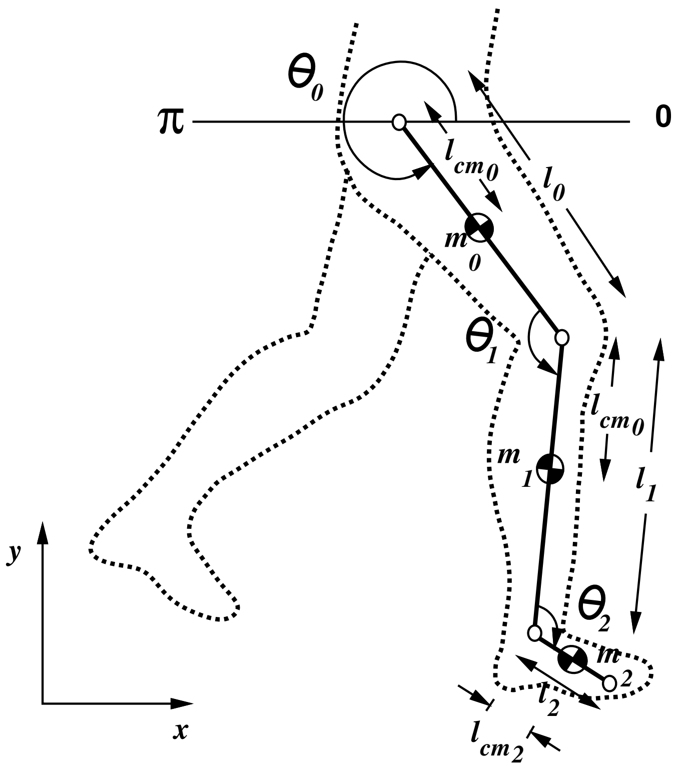

Figure 6: Geometry of the Simulated Human Leg.

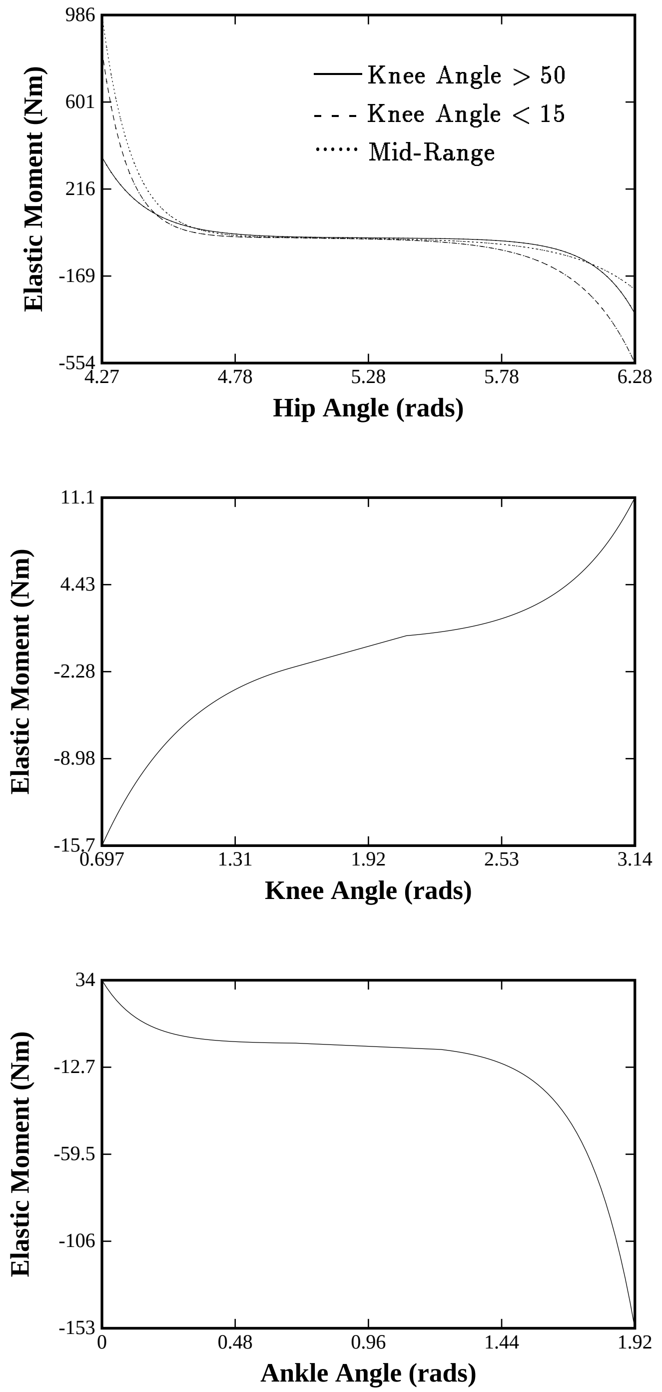

Figure 7: Elastic Moment about the hip, knee, (adapted from (Yoon and Mansour, 1982; Mansour and Audu, 1986)) and ankle joints.

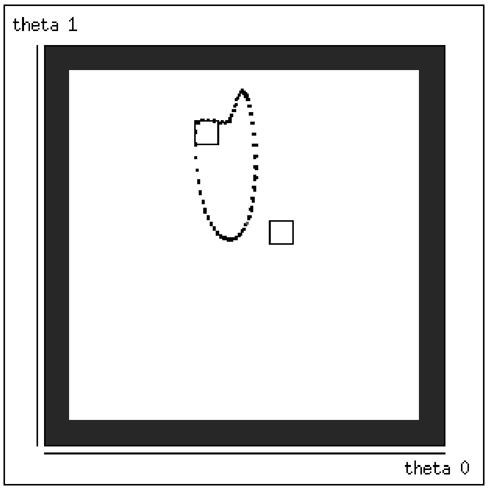

Figure 8: Monoped constant-energy orbit in configuration space.

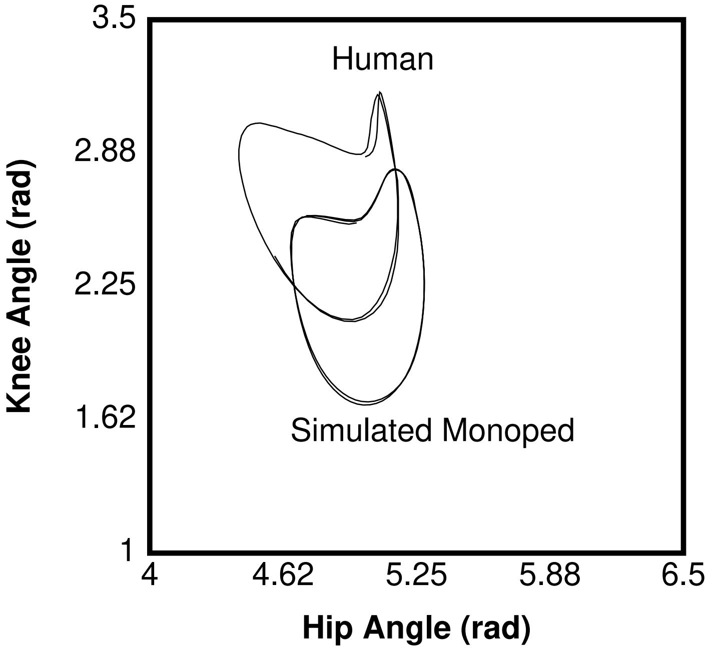

Figure 9: Comparison of the angle-angle diagram for the human subject and the dynamically equivalent leg simulation.